Analysis of the Shear Characteristics of a Deep, Anchored Rock Mass Under Creep Fatigue Loading

Xiaofeng Li (lixiaofeng19902021@163.com)
Liaoning Technical University
Zhixiang Yin
Liaoning Technical University

Research Article

Keywords: bolted rock mass, creep fatigue load, shear creep, shear modulus, creep fatigue model

Posted Date: July 1st, 2021

DOI: https://doi.org/10.21203/rs.3.rs-668378/v1

Analysis of the shear characteristics of a deep, anchored rock mass under creep fatigue loading

Xiaofeng Li*, Zhixiang Yin

[1]Department of Civil Engineering, Liaoning Technical University, Fuxin, 123000, China;

Corresponding Author E-mail:lixiaofeng19902021@163.com

Abstract: To study the influence of earthquakes and engineering disturbances on the deformation of deeply buried rock masses, shear tests were carried out on sandstone, marble and granite anchored specimens under creep fatigue loading, and a new creep fatigue model was established to characterize the deformation characteristics of anchored rock masses under creep fatigue loading. The creep fatigue curves of different lithologies clearly show three stages: creep attenuation, steady-state creep and accelerated creep. Fatigue loading can increase the creep of anchored specimens, and the lower the rock strength is, the higher the creep variable under fatigue loading. However, for the same rock strength, with the increase in load level, the creep variable produced by creep fatigue load presents a linear downward trend. Considering the changes in the mechanical properties of the anchored rock mass under creep fatigue loading, the creep fatigue model of anchored rock masses is established by introducing a function of the fatigue shear modulus, and the accuracy and applicability of the model are verified by laboratory creep fatigue test data. The model provides a theoretical basis for the study of anchored rock mass support under low-frequency earthquakes or blasting loads.

Key words: bolted rock mass; creep fatigue load; shear creep; shear modulus; creep fatigue model

Introduction

In the construction of strategic projects in large-scale deep rock masses in China, the safety and stability of underground engineering are of great importance. Complex engineering geological environments have presented many challenges in the development of underground engineering [1-3]. For example, the engineering construction of the Sichuan-Tibet railway is particularly challenging because the railway corridor is formed under the coupling effect of structural activity, geomorphic uplift, climate change and engineering disturbance[4,5]. The structural deformation, rock mass loosening, surface freeze-thaw and engineering disturbance in the shallow crust along the corridor have a profound impact on the stability of the geological body, engineering geological body, engineering rock soil mass and engineering structure body in the corridor area. The Sichuan-Tibet railway passes through complex geological structures [6-8].

Scholars in China and abroad have performed a considerable amount of research on the shear creep of rock. Liu Yan et al. [9,10]took the shear creep characteristics of mica schist as a research object and discussed the variation law of the radial displacement of mica schist with time determined from the results of the indoor shear creep tests of mica schist. To study the shear creep characteristics of marble with structural planes, He et al. [11]carried out a series of shear creep tests on two kinds of marble with weak and hard structural planes. To study the influence of weak intercalation on the long-term stability of geological bodies, Yao et al. [12]proposed a new unsteady fractal differential creep (UFDC) model based on fractal derivative theory and the results of circumferential shear creep tests of weak interlayers to effectively explain the creep deformation of soft interlayers. Zhang Fengrui et al. [13]carried out a series of shear creep tests of serrated structural planes under various pore water pressures to explore the influence of pore water pressure on the

shear creep characteristics of rock mass discontinuities.

Additionally, experts have carried out corresponding research on the rheological properties of rocks under different conditions. Wu et al. [14]conducted shear creep tests on fractured mudstone to study the influence of normal stress and precut fracture length on the shear creep characteristics of mudstone. Because most creep models cannot accurately describe the nonlinear creep behavior of mudstone, an improved time-varying creep model was proposed. Zhang Zelin et al. [15]carried out creep tests of mudstone under different loading modes and water contents and established an appropriate creep model. Zhang Fengrui et al. [16]carried out shear creep tests on samples after different numbers of freeze-thaw cycles to study the influence of freeze-thaw cycling on the shear creep characteristics of rock. Chen Weizhong et al. [17]carried out a series of long-term creep tests of clay rock under different confining pressures and deviatoric stresses under complex conditions of thermal-fluid-mechanical coupling. Xu et al. [18]carried out a series of shear creep tests on rocks with discontinuities to simulate the initiation and propagation of cracks under the action of continuous shear stress and normal stress. Jia et al. [19]carried out shear creep tests on structural plane faults and established a corresponding creep formula.

The above research mainly analyzes the rock mass from the aspects of freeze-thaw cycles and structural planes. Research on the influence of fatigue loads caused by low-frequency earthquakes or blasting on the rheological properties of rock is relatively limited, while the occurrence frequency of low-frequency earthquakes in actual geotechnical engineering is relatively high, and the impact on geotechnical engineering is also important [20-22]. Earthquakes occur frequently along the Sichuan-Tibet railway, and fault and fracture zones are relatively dense. Earthquakes and engineering blasting result in both dynamic and cyclic loads that are described as low-cycle fatigue loads [23,24]. Based on the above engineering background, to study the shear characteristics of deep anchored jointed rock masses under creep fatigue loading, the deformation characteristics of anchored rock masses under creep fatigue loading under different rock strengths are analyzed through laboratory tests. Based on the change in shear modulus under fatigue loading, a constitutive model reflecting creep fatigue loading is constructed, and the accuracy of the model is verified. This model can comprehensively explain the shear failure characteristics and anchoring mechanism of anchored jointed rock masses under complex stress paths and provide a reference for the study of deep rock mass disaster prevention and safety production.

Creep fatigue testing

Specimen preparation

The test rock samples include sandstone, marble and granite, and the test pieces are all 100 mm × 100 mm × 100 mm cubes. The size of the test pieces conforms to the relevant provisions of the test specifications of the International Society of Rock Mechanics [25,26]. The steps followed to prepare the test pieces are as follows:

(1) Rock block processing: A massive rock mass is selected, a rock cutter is used to process the rock block into a 100 mm × 100 mm × 50 mm rock mass, and a drilling machine is used to drill a hole with a diameter of 10 mm and length of 50 mm from the center of a side with dimensions of 100 mm × 100 mm (for the anchor rod).

(2) Rock block bonding: The joints are used to bond the upper and lower plates of the rock block. A joint is made by pouring cement mortar into a of 100 mm × 100 mm × 5 mm space (the joint thickness is 5 mm). The joint mix ratio is cement:river sand:water = 1:1.5:0.8. The test materials are 42.5 ordinary silicate cement and medium-grained sand. The joint shape, size and material distribution are checked during the test. The indoor curing time is 28 days.

(3) Installation of the anchor rod: HRB335 steel with a yield strength of 335 MPa is selected as the

anchor material. A steel bar with a diameter of 6 mm is placed in the hole in the test piece. The overall length of the reinforcement is 110 mm. The exposed end of the ribbed steel bar is machined to a length of 10 mm, and 50 mm extends into the test piece, through both the upper and lower walls. Grouting is used to fill the holes and reinforce the anchor rod. The grouting material is the same as the joint material.

An anchored rock mass fabricated according to the above steps is shown in Fig. 1:

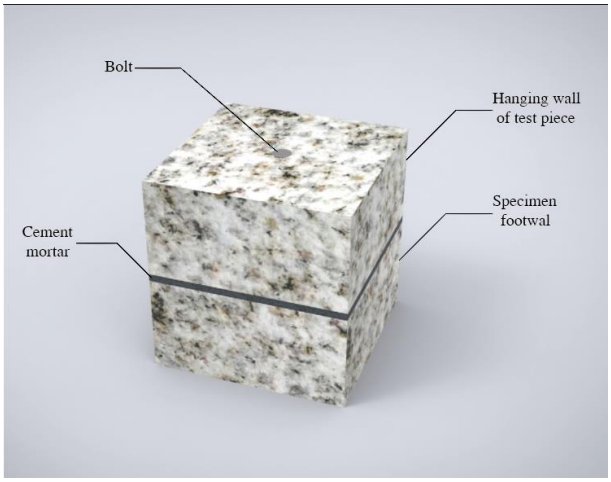

(a) Model diagram

(b) Physical picture

Figure. 1 Diagram and photograph of test pieces

The test loading system adopts the cutting equipment of the TAW-2000 triaxial testing servo apparatus of the civil engineering test center of Liaoning University of Engineering and Technology, as shown in Fig. 2. It is mainly composed of a loading system, measuring system and controller. Fully automatic control is achieved by microcomputer-controlled electrohydraulic servo valve loading and manual hydraulic loading. The host machine and the control cabinet are separate. The testing machine uses sensors to measure force, and the host machine automatically collects stress data and displacement. The resulting test curves and test results have high reliability.

Figure. 2 Shearing device

Test scheme and steps

Test scheme Before the test, it was necessary to determine the basic mechanical parameters, such as compressive strength, tensile strength and elastic modulus, of the three rock materials. The basic mechanical parameters of the three kinds of rocks were determined by uniaxial compression tests and Brazilian splitting tests [27,28], and the details are shown in Table 1:

Rock specimen	Compressive strength (MPa)	Tensile strength (MPa)	Elastic modulus (GPa)	Poisson's ratio	Cohesion (MPa)	Internal friction angle (°)
Sandstone	30.20	1.42	7.83	0.31	8.11	35.12
Marble	110.70	3.79	20.20	0.28	15.12	33.50
Granite	120.23	4.11	23.10	0.22	14.13	45.03

Table 1 Conventional mechanical parameters of the rock mass

During these tests, the loading rate was set to 200 N/s, the fatigue load was set to ± 5 kN on the basis of all levels of loading, and the shear stress was set to ± 0.5 MPa. The load amplitude was 1/10-1/100 of the compressive strength. The specific test scheme is shown in Fig. 3.

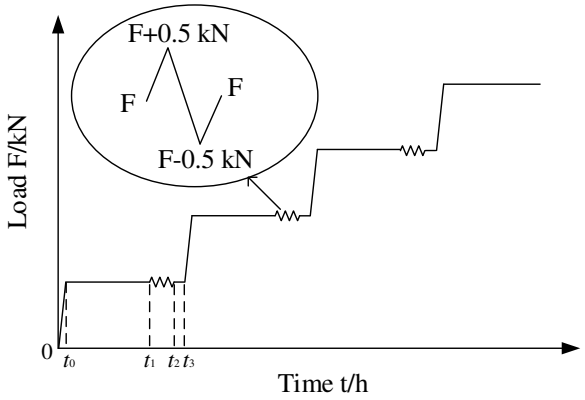

Figure. 3 Loading path diagram

Note: 0-t_0 is the loading time before reaching the specified load; t_0-t_1 is the specified load stabilization time; t_1-t_2 is the fatigue load application time; and t_2-t_3 is the stability time after the fatigue load is applied.

Test procedure The creep fatigue testing was carried out by graded loading, to approximately 20%, 40%, 60% and 80% of the compressive strength of the specimen, i.e., 2 MPa, 4 MPa, 6 MPa and 8 MPa. This test is an unconfined shear test, and the relevant test steps are as follows:

(1) Application of shear stress: The specimen is put into the shear device, and then the load is controlled at a rate of 0.5 MPa/s to the specified shear stress, which is then maintained.

(2) Application of fatigue load: When the shear stress of each level is applied for approximately 59 h, load control is adopted, and fatigue loading is applied at a rate of 200 N/s. Before and after the fatigue loading is applied, the pressure is stabilized for a certain period, and the internal stress of the specimen is adjusted to make the conditions more accurately match those encountered in engineering practice. The test is carried out according to the above steps until the specimen is damaged.

(3) Reading data: The shear creep values are read at intervals of 5 min, 10 min, 20 min, 40 min, 1 h, 2 h, 4 h, 8 h and 12 h during the creep attenuation and steady-state creep stages and then read every 12 h until the end of the test. During the fatigue loading stage and creep acceleration stage, the data are read every 0.5 min. The condition for the stability of the shear creep deformation of a rock mass is a creep rate increment $\leq 5\times10^{-4}$ mm/D[29].

Analysis of the creep fatigue curves

Analysis of the test curves

To explore the shear mechanical properties of different rock strengths under creep fatigue loading, typical test data were selected to draw the curves of strain and stress with time for the different rock types, as shown in Fig. 4:

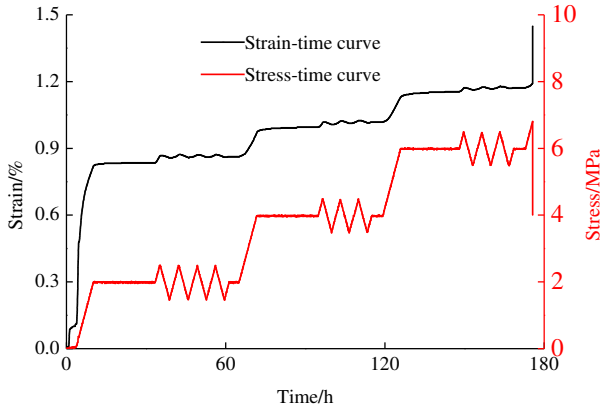

(a) Sandstone

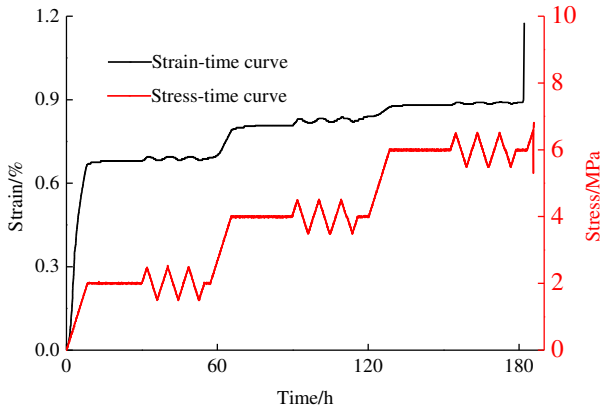

(b) Marble

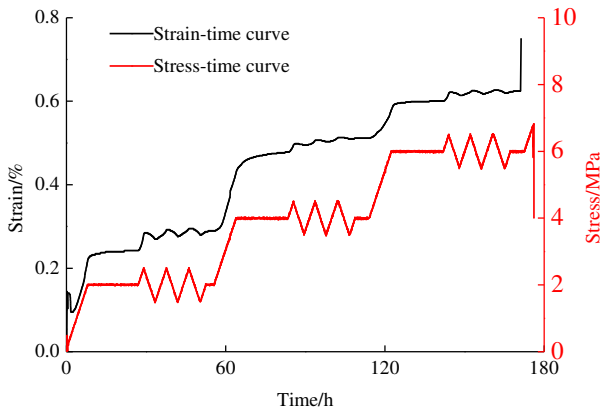

(c) Granite

Figure. 4 Time-dependent curves of strain and stress under different rock strengths

Due to the different rock strengths, the test curves measured during the creep fatigue loading tests are different, but they all have three typical stages, namely, a creep attenuation stage, a steady-state creep stage and an accelerated creep stage; when a specimen is in the steady-state stage, with the application of fatigue loading, the creep curve will fluctuate to a certain extent, that is, with the increase or decrease in stress, the creep curve will fluctuate. The results show that the change in the shear strain lags behind the change in the shear stress, which indicates that the rock has an elastic aftereffect. The steady creep curve of each stage is amplified to some extent compared with that before the fatigue loading is applied, which is due to the microcracks present in each specimen during the steady-state stage, causing the rock to crack under the action of fatigue loading. As a result, the deformation of a specimen is greater after fatigue loading is applied.

Creep analysis

Creep deformation To quantitatively analyze the influence of fatigue loading on shear creep at all levels, the steady creep variables of each stage under different rock strengths are determined, as shown in Fig. 5:

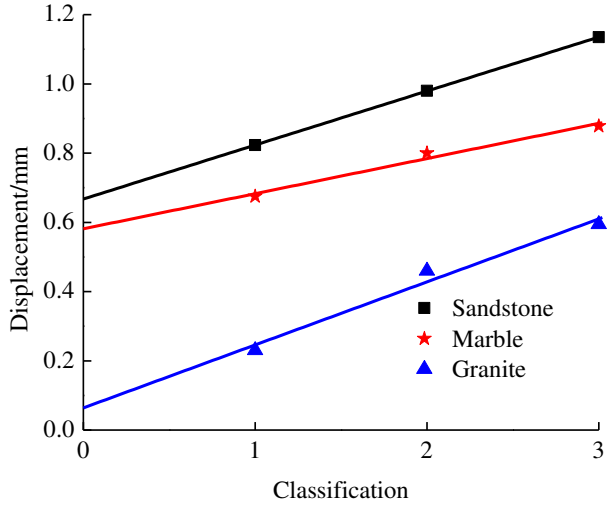

Figure. 5 Fitting curve of creep at different stages

$$y = M + N * x \tag{1}$$

In this formula, M and N are the relevant parameters of the formula, x is the load level, and the relevant fitting parameters are shown in Table 2.

Rock specimen	M	N	R^2
Sandstone	0.667	0.156	1
Marble	0.581	0.102	0.965

Granite	0.064	0.182	0.955

Table 2 Related parameters of the fitting curve

The creep variable increases with the grading under different rock strengths. The creep variables ordered from large to small correspond to sandstone, marble, and granite, and the coefficient of fit is higher than 0.95. This finding indicates that the creep and grading show a linear relationship under different rock strengths; in formula (1), *M* is the intercept of the fitting formula on the Y axis, which is defined as the instantaneous creep intercept, which can characterize the instantaneous creep of the specimen, and the order of the sizes of the instantaneous creep intercepts under the different rock strengths is sandstone>marble>granite. The higher the rock strength is, the stronger its ability to resist shear deformation and the lower the instantaneous creep; consequently, the instantaneous creep intercept *M* is smaller. *N* is the slope of the fitting formula (1) and represents the initial creep rate in the steady-state phase. The larger *N* is, the faster the change in the initial creep in the steady state stage; the corresponding order is granite>sandstone>marble. Since the change in creep during the steady-state stage is small, the deformation of a rock specimen in the steady-state stage can be quantitatively reflected by the change in *N*.

Creep fatigue increment To study the influence of fatigue loading on the shear creep deformation of rock specimens at all levels of loading, the creep variables before and after the application of fatigue loads are summarized and plotted, as shown in Fig. 6. The changes in creep increment during different stages before and after fatigue loading are plotted as shown in Fig. 7:

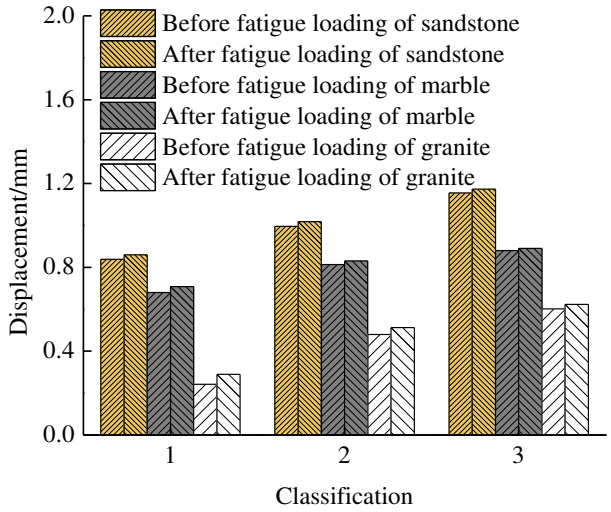

Figure. 6 Bar chart of creep before and after fatigue loading

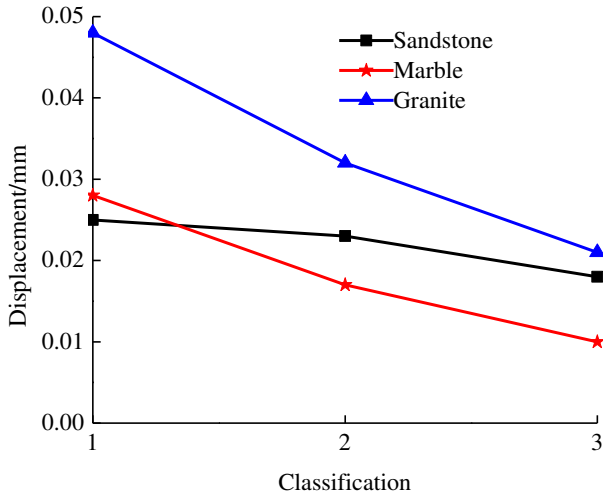

Figure. 7 Creep increment curve before and after fatigue loading

The creep variables before and after fatigue at all levels of loading follow the order of sandstone >

marble > granite, which indicates that the creep variables under shear loads of different rock strengths are different. The lower the rock strength is, the larger the creep variable is, and vice versa. From the results of the creep increment before and after fatigue loading is applied at all levels, the overall creep variable decreases with increasing load level, indicating that the creep increment increases. The results show that the sensitivity of fatigue loading to shear creep decreases with the increase in load level, which is due to the increase in shear stress, leading to further compaction of the specimen and a decrease in the creep variable. Compared with the incremental change in the sandstone, the incremental changes in the marble and granite have larger ranges, indicating that the influence of fatigue loading on the deformation of high-strength rock is more obvious than that on weak rock.

Shear modulus

As a variable describing the inherent properties of rock, the shear modulus is often used to characterize the change in rock strength [6,30]. To explore the effect of fatigue loading on the shear modulus of the specimen, the shear modulus change curve with time throughout the creep process is drawn, as shown in Fig. 8.

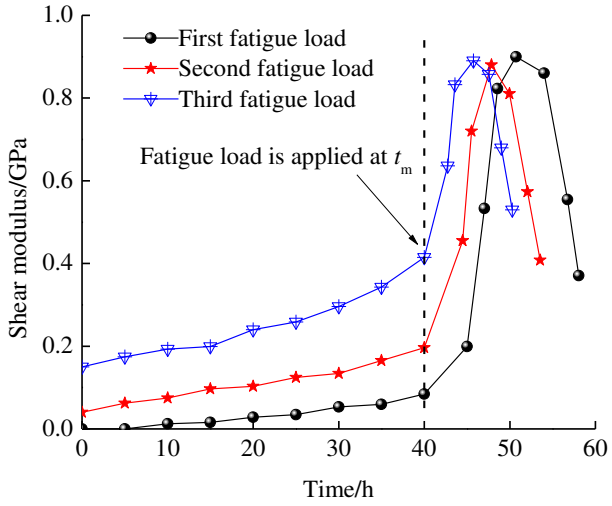

(a) Sandstone

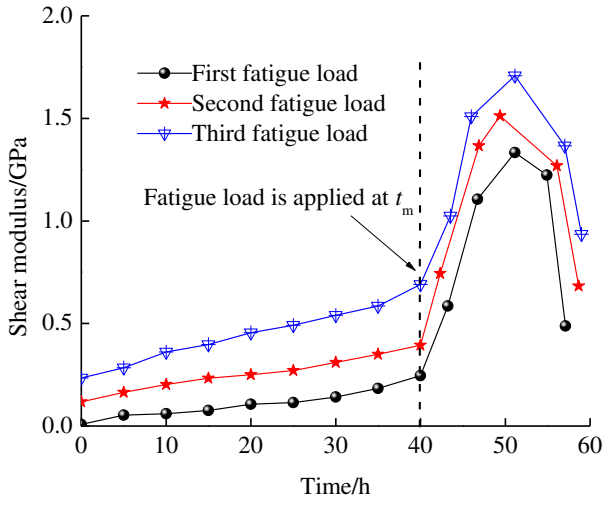

(b) Marble

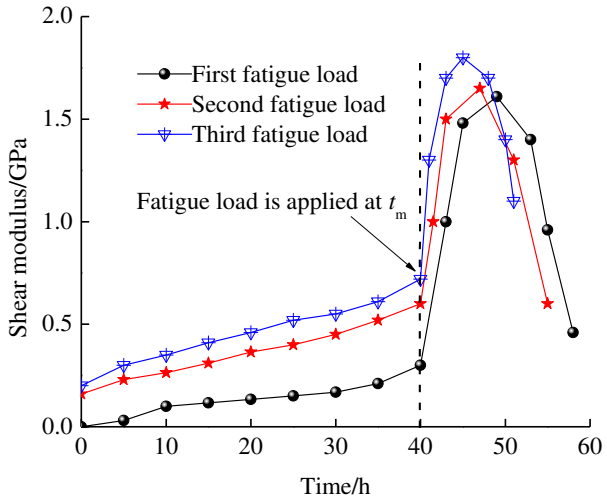

(c) Granite

Figure. 8 Shear modulus versus time curve

Fig. 8 shows that the shear modulus changes piecewise with time. Before the fatigue load is applied, the curve changes approximately linearly, while after the fatigue load is applied, the curve shows a nonlinear change trend, which is represented by a piecewise function:

$$G(t-t_m)=\begin{cases} a_1 t+b_1 & (t\le t_m) \\ a_2 t^2+b_2 t+c & (t>t_m) \end{cases} \tag{2}$$

where $G_1(t\text{-}t_m)$ is the function of fatigue shear modulus; t_m is the initial moment of fatigue load application, which is 40 h; a_1 and b_1 are the coefficients of the first-order function; and a_2, b_2 and c are the coefficients of the quadratic function. Regression analysis of equation (2) is carried out using the data in Fig. 8, as shown in Table 3.

Rock specimen	Load level	First-order function			Quadratic function			
		a_1	b_1	R_1^2	a_2	b_2	c	R_2^2
Sandstone	1	0.02	-0.09	0.94	-0.02	1.60	-40.69	0.98
	2	0.03	0.39	0.97	-0.02	2.03	-48.55	0.90
	3	0.06	0.13	0.93	-0.02	1.95	-44.03	0.90
Marble	1	0.01	0.01	0.93	-0.02	1.72	-41.91	0.80
	2	0.01	0.13	0.98	-0.01	1.25	-29.96	0.95
	3	0.01	0.24	0.99	-0.01	1.29	-31.10	0.94
Granite	1	0.01	0.01	0.93	-0.01	1.46	-34.14	0.94
	2	0.01	0.16	0.99	-0.02	1.61	-36.34	0.89
	3	0.01	0.22	0.98	-0.02	2.27	-50.00	0.98

Table 3 Related parameters of fitting curve

Creep fatigue modeling

Creep model

The creep curve of a rock mass mainly includes three stages [31,32]. The model of a combination of elastic elements, viscoelastic elements and viscoplastic elements in series is often used to describe the creep attenuation and steady-state creep stages. The creep model is shown in Fig. 9 [33]:

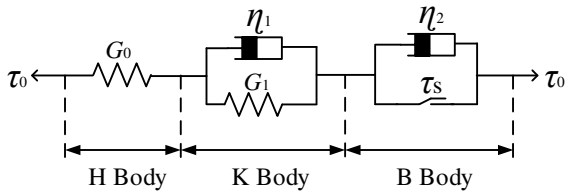

Figure. 9 Shear creep model

In Fig. 9, G_0 is the instantaneous shear modulus, G_1 is the viscoelastic shear modulus, and η_1 and η_2 are the viscosity coefficients, which indicate that the speed of the rheological change is stable. The smaller the value of a viscosity coefficient is, the shorter the time to reach stability. τ_s is the yield shear stress or long-term shear strength; τ_0 is the shear stress.

Considering the actual stress of the rock mass, the model was modified as follows:

(1) The above analysis shows that the creep attenuation stage has obvious nonlinear characteristics and that the Kelvin model cannot describe the creep attenuation stage of rock. Considering the time correlation of the viscosity coefficient in the Kelvin model, assuming that the coefficient satisfies the power function relationship with time in the creep process, the nonlinear Kelvin viscoelastic model is established.

(2) To satisfy the shear rheological properties of specimens under fatigue loading, a modified nonlinear Kelvin model is obtained by introducing the fatigue shear modulus function $G_1(t\text{-}t_m)$.

(3) When the stress level imposed by the creep test is higher than the long-term strength, body B plays a role. The steady-state stage can be described as a stable creep stage, but the unstable creep stage and accelerated creep stage cannot be well described. This problem can be solved by connecting a nonlinear rheological element E with the time factor in series. The model of body E is shown in Fig. 10 [34,35]:

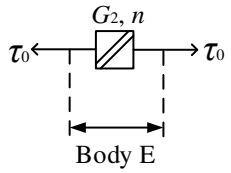

Figure. 10 Model of body E

$$\gamma=\begin{cases}0 \ \ (t\le t_2)\\ \dfrac{\tau_0}{G_2}\left\{1-\exp\left[-\left(\dfrac{t-t_2}{t_3-t_2}\right)^n\right]\right\} \ \ (t>t_2)\end{cases} \qquad (3)$$

where G_2 and n are model parameters, γ is the shear strain, t_2 is the start time of the acceleration stage, and t_3 is the end time of the acceleration stage.

Creep fatigue model

The creep fatigue model is shown in Fig 11, and the corresponding creep equation is as follows:

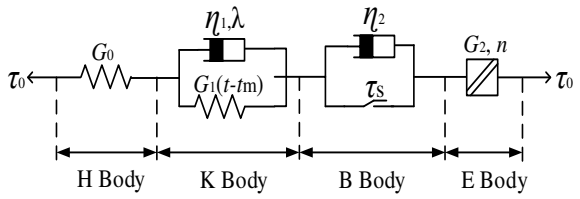

Figure. 11 Creep fatigue model

In this figure, λ is a constant, and $G_1(t\text{-}t_m)$ is a function of the viscoelastic fatigue shear modulus varying with time.

(1) When the shear stress level is less than the long-term strength, the creep equation is as follows:

$$\gamma = \frac{\tau_0}{G_0} + \frac{\tau_0}{G_1(t-t_m)}\left[1-\exp(-\frac{G_1(t-t_m)}{\eta_1\lambda}t^{\lambda})\right] \tag{4}$$

(2) When the shear stress level is higher than the long-term strength but creep has not reached the acceleration stage, the creep equation is as follows:

$$\gamma = \frac{\tau_0}{G_0} + \frac{\tau_0}{G_1(t-t_m)}\left[1-\exp(-\frac{G_1(t-t_m)}{\eta_1\lambda}t^{\lambda})\right] + \frac{\tau_0-\tau_S}{\eta_2}t \tag{5}$$

(3) When the shear stress level is higher than the long-term strength and the creep reaches the acceleration stage, the creep equation is as follows:

$$\gamma = \frac{\tau_0}{G_0} + \frac{\tau_0}{G_1(t-t_m)}\left[1-\exp(-\frac{G_1(t-t_m)}{\eta_1\lambda}t^{\lambda})\right] + \frac{\tau_0-\tau_S}{\eta_2}t + \frac{\tau_0}{G_2}\left\{1-\exp\left[-(\frac{t-t_2}{t_3-t_2})^n\right]\right\} \tag{6}$$

In conclusion, the shear creep equation under fatigue loading is as follows:

$$\gamma=\begin{cases} \dfrac{\tau_0}{G_0} + \dfrac{\tau_0}{G_1(t-t_m)}\left[1-\exp(-\dfrac{G_1(t-t_m)}{\eta_1\lambda}t^{\lambda})\right] & (\tau_0 \le \tau_S) \\ \dfrac{\tau_0}{G_0} + \dfrac{\tau_0}{G_1(t-t_m)}\left[1-\exp(-\dfrac{G_1(t-t_m)}{\eta_1\lambda}t^{\lambda})\right] + \dfrac{\tau_0-\tau_S}{\eta_2}t & (\tau_0 > \tau_S, t \le t_2) \\ \dfrac{\tau_0}{G_0} + \dfrac{\tau_0}{G_1(t-t_m)}\left[1-\exp(-\dfrac{G_1(t-t_m)}{\eta_1\lambda}t^{\lambda})\right] + \dfrac{\tau_0-\tau_S}{\eta_2}t + \dfrac{\tau_0}{G_2}\left\{1-\exp\left[-(\dfrac{t-t_2}{t_3-t_2})^n\right]\right\} & (\tau_0 > \tau_S, t > t_2) \end{cases} \tag{7}$$

Model validation

To solve the relevant parameters of the creep equation, combined with the creep test data, the mathematical optimization software 1stOpt is used; based on the quasi-Newton method and general global optimization method [36,37], the solution method of equation (7) is given under different conditions, as shown in Table 4:

Specimen	Shear stress (MPa)	G_0 (GPa)	G_1 (GPa)	η_1 (GPa·h)	η_2 (GPa·h)	λ	G_2 (GPa)	n	R^2
Sandstone	2	1.47	23.41	11.54	0.21	0.74			
	4	1.22	20.17	10.13	1.42	0.82			
	6	0.99	18.52	9.77	0.63	0.91			
	6.5	0.86	15.44	8.12	0.77	0.21	10.04	0.58	0.951
Marble	2	0.73	14.97	7.46	0.84	0.44			
	4	2.31	34.22	16.52	1.09	0.56			
	6	2.14	30.56	12.44	1.54	0.84			
	6.4	1.98	28.94	10.12	0.13	0.11	15.43	0.66	0.944
Granite	2	1.87	25.10	9.81	0.15	0.37			
	4	1.74	24.13	9.54	3.11	0.59			
	6	0.44	47.18	19.46	2.56	0.87			
	6.6	1.12	45.69	18.57	1.69	0.14	22.16	0.74	0.936

Table 4 Summary of model parameters

The shear creep model under fatigue loading can be obtained by introducing the relevant parameters in Table 4 into equation (7). To verify the accuracy of the model, comparison diagrams between the test data

and the theoretical curves are drawn, as shown in Fig. 12:

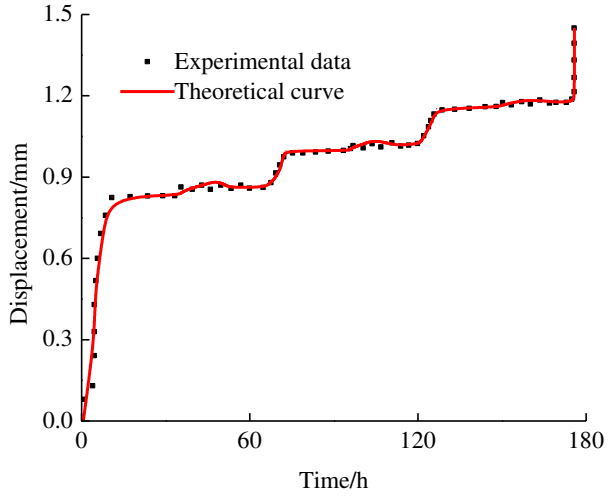

(a) Sandstone

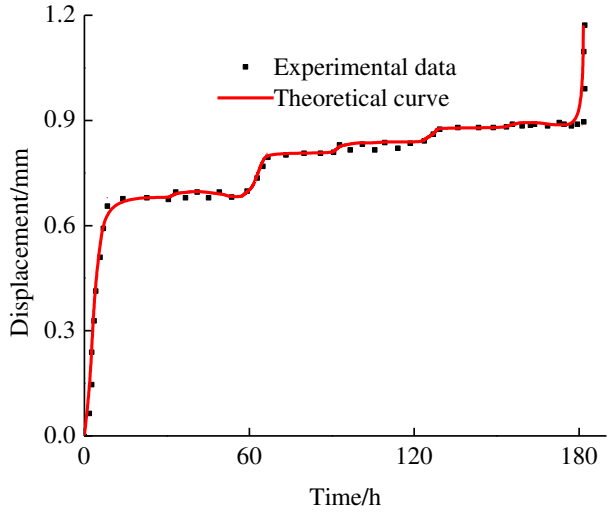

(b) Marble

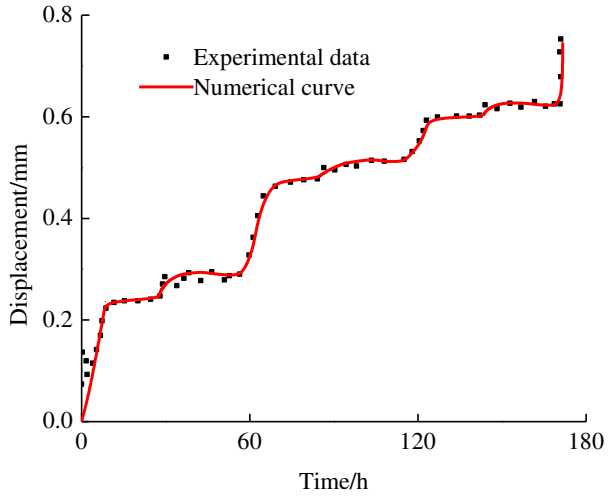

(c) Granite

Figure. 12 Comparisons between the experimental data and theoretical curves

The theoretical curves can accurately describe the creep test results and can better describe the resulting fatigue curves. Generally, the fitting coefficient is higher than 0.93, indicating that the fitting degree is good, which indicates that the model can accurately reflect the shear mechanical characteristics of anchored rock masses under creep fatigue loading.

Conclusion

In this paper, through the shear testing of anchored rock masses with different rock strengths under creep fatigue loading, the influence law of fatigue loading on shear creep is explored:

(1) The creep fatigue tests under different rock strengths exhibit typical creep mechanical properties, namely, instantaneous creep, attenuation creep, steady-state creep and accelerated creep. With increasing specimen strength, the unstable creep stage appears earlier. Additionally, the creep variable increases with increasing load level under different rock strengths; the creep variable values exhibit the order of sandstone > marble > granite.

(2) By applying fatigue loading during shear creep tests, the resulting creep curve fluctuates to a certain extent; that is, with the increase and decrease in stress, the strain fluctuates, and the fluctuation in strain occurs after the change in stress, which indicates that the change in shear strain lags behind the change in shear stress. The creep increment under fatigue loading presents a linearly decreasing trend with progression of the creep stages, and the sensitivity of fatigue loading to shear creep decreases with the increase in load level.

(3) Considering the influence of fatigue loading on the model parameters, the fatigue shear modulus function is introduced into the Kelvin model, and a creep fatigue model based on fatigue loading is constructed. The accuracy of the model is verified by comparing the test data with the theoretical curve, which provides the basis for the support of the surrounding rock cavern under low-frequency seismic loading.

Acknowledgements

We gratefully acknowledged the National Natural Science Foundation of China (51774173) for funding this work. Special thanks are given to Professor Xiangzhi Yin for providing technical support. I declare that this paper has been presented as preprint in Research Square.

Data availability

The data used to support the findings of this study are available from the corresponding author upon request.

Conflict of interest statement

We declare that we have no financial and personal relationships with other people or organizations that can inappropriately influence our work, there is no professional or other personal interest of any nature or kind in any product, service and/or company that could be construed as influencing the position presented in, or the review of, the manuscript entitled, “Analysis of the shear characteristics of a deep, anchored rock mass under creep fatigue loading”.

References

1 Xie, H. Research review of the state key research development program of China:Deep rock mechanics and mining theory. *J China Coal Soc* **44**, 1283-1305, doi:10.13225 /j.cnki.jccs.2019.6038 (2019).

2 Tan, Z. *et al.* Differentiation characteristics of insitu stress in deep rock. *Chin J Rock Mech Eng* **38**, 58-65,

doi:10.13722/j.cnki.jrme.2019.0307 (2019).

3 Zhu, G. *et al.* Experimental Study to Design an Analog Material for Jinping Marble with High Strength, High Brittleness and High Unit Weight and Ductility. *Rock Mech Rock Eng* **52**, 2279-2292, doi:10.1007/s00603-018-1710-z (2019).

4 Urai, J. L., Spiers, C. J., Zwart, H. J. & Lister, G. S. Weakening of rock salt by water during long-term creep. *Nature* **324**, 554-557, doi:10.1038/324554a0 (1986).

5 Jin, J., Li, S., Song, C., Zhang, X. & Lv, X. Ageing deformation of tailings dams in seasonally frozen soil areas under freeze-thaw cycles. *Scientific Reports* **9**, 150-158 (2019).

6 Wang, J., Liang, B. & Yang, P. Creep experiment and nonlinear disturbance creep model of gneiss under dynamic and static loads. *J China Coal Soc* **44**, 199-205, doi:10.13225/ j.cnki. jccs. 2018.5036 (2019).

7 Xie, H. *et al.* Theoretical and technological conception of the fluidization mining for deep coal resources. *J China Coal Soc* **42**, 547-556, doi:10.13225/j.cnki.jccs.2017.0299 (2017).

8 Demir, S. & Özener, P. Numerical investigation of seismic performance of high modulus columns under earthquake loading. *Earthquake Engineering and Engineering Vibration* **18**, 811-822, doi:10.1007/s11803-019-0537-2 (2019).

9 Liu, T. Experimental study on shear creep characteristics of mica schist. *Geotechnical Investigation & Surveying* **48**, 17-23, doi:CNKI:SUN:GCKC.0.2020-02-004 (2020).

10 Hudson, J. A. Effect of Time on the Mechanical Behaviour of Failed Rock. *Nature* **232**, 185-189, doi:10.1038/232185a0 (1971).

11 He, Z., Zhu, Z., Ni, X. & Li, Z. Shear creep tests and creep constitutive model of marble with structural plane. *European Journal of Environmental and Civil Engineering* **23**, 1275-1293, doi:10.1080/19648189.2017.1347066 (2017).

12 Yao, W., Hu, B., Zhan, H., Ma, C. & Zhao, N. A Novel Unsteady Fractal Derivative Creep Model for Soft Interlayers with Varying Water Contents. *KSCE Journal of Civil Engineering* **23**, 5064-5075, doi:10.1007/s12205-019-1820-5 (2019).

13 Zhang, F., Jiang, Z. & Yang, X. Effect of pore water pressure on shear creep characteristics of serrate structural plane. *Rock Soil Mech* **41**, 2901-2912, doi:10.16285/j.rsm.2019.1907 (2020).

14 Wu, L., Li, S., Sun, P., Huang, R. & Li, B. Shear Creep Tests on Fissured Mudstone and an Improved Time-Dependent Model. *Pure and Applied Geophysics* **176**, 4797-4808, doi:10.1007/s00024-019-02257-6 (2019).

15 Zhang, Z., Wu, S., Wang, T., Xin, P. & Liang, C. Study on shear creep behavior and its model of mudstone in Tianshui, Gansu Province. *Chin J Rock Mech Eng* **38**, 331-345, doi:10.13722/j.cnki.jrme.2018.1518 (2019).

16 Zhang, F., Jiang, Z., Yang, X. & Shen, F. Experimental and model study on shear creep of granite under freeze-thaw cycles. *Rock Soil Mech* **41**, 153-163 (2020).

17 Chen, W., Li, F., Lei, J., Yu, H. & Ma, Y. Study on creep characteristics of claystone under thermo-hydro-mechanical coupling. *Rock Soil Mech* **41**, 23-32, doi:10.16285/j.rsm.2019.0016 (2020).

18 Xu, T., Xu, Q., Tang, C.-a. & Ranjith, P. G. The evolution of rock failure with discontinuities due to shear creep. *Acta Geotech* **8**, 567-581, doi:10.1007/s11440-013-0244-5 (2013).

19 Jia, C., Xu, W. Y., Wang, R., Wang, S. & Lin, Z. Experimental investigation on shear creep properties of

undisturbed rock discontinuity in Baihetan Hydropower Station. *Int J Rock Mech Min* **104**, 27-33, doi:10.1016/j.ijrmms.2018.02.011 (2018).

20 Gao, M. *et al.* In-situ disturbed mechanical behavior of deep coal rock. *J China Coal Soc* **45**, 2691-2703, doi:10.13225/j.cnki.jccs.2020.0784 (2020).

21 Gao, M., Jin, W., Zheng, C. & Zhou, H. Real-time evolution and connectivity of mined crack network. *J China Coal Soc* **37**, 1535-1540, doi:10.1007/s11783-011-0280-z (2012).

22 Wang, J.-g., Sun, Q.-l., Liang, B., Yang, P.-j. & Yu, Q.-r. Mudstone creep experiment and nonlinear damage model study under cyclic disturbance load. *Scientific Reports* **10**, 9305-9311, doi:10.1038/s41598-020-66245-w (2020).

23 Farahi, M. & Erfani, S. Efficiency of employing fiber-based finite-length plastic hinges in simulating the cyclic and seismic behavior of steel hollow columns compared with other common modelling approaches. *Earthquake Engineering and Engineering Vibration* **18**, 777-794, doi:10.1007/s11803-019-0536-3 (2019).

24 Fermandois, G. A. & Spencer, B. F. Model-based framework for multi-axial real-time hybrid simulation testing. *Earthquake Engineering and Engineering Vibration* **16**, 671-691, doi:10.1007/s11803-017-0407-8 (2017).

25 Riock, M. Suggested methods for determining the strength of rock materials in triaxial compression. *Int. J. Rock Mech. Min. Sci. & Gcomech. Abstr* **15**, 47-51, doi:10.1016/0148-9062(83)90598-3 (1978).

26 Saha, R., Haldar, S. & Dutta, S. C. Influence of dynamic soil-pile raft-structure interaction: an experimental approach. *Earthquake Engineering and Engineering Vibration* **14**, 625-645, doi:10.1007/s11803-015-0050-1 (2015).

27 Melbouci, B., Bahar, R. & Cambou, B. Study of the behaviour of schist grains under crushing. *B Eng Geol Environ* **67**, 209-218, doi:10.1007/s10064-008-0125-6 (2008).

28 Yang, S.-Q. & Hu, B. Creep and permeability evolution behavior of red sandstone containing a single fissure under a confining pressure of 30 MPa. *Scientific Reports* **10**, 1900-1906, doi:10.1038/s41598-020-58595-2 (2020).

29 Peng, R., Xue, D., Huafei, S. & Zhou, H. Characteristics of strong disturbance to rock mass in deep mining. *J China Coal Soc* **44**, 1359-1368, doi:10.13225/j.cnki.jccs.2019.6024 (2019).

30 Sahu, L. & Dey, S. Enrichment of carbon recovery of high ash coal fines using air fluidized vibratory deck separator. *Int J Coal Sci Technol* **4**, 262-273, doi:10.1007/s40789-017-0172-3 (2017).

31 Ozhan, H. O. & Guler, E. Critical Tendon Bond Length for Prestressed Ground Anchors in Pullout Performance Tests Conducted in Sand. *International Journal of Civil Engineering* **16**, 1329-1340, doi:10.1007/s40999-017-0261-0 (2018).

32 Mishra, V. & Singh, K. N. Microstructural relation of macerals with mineral matter in coals from Ib valley and Umaria, Son-Mahanadi basin, India. *Int J Coal Sci Technol* **4**, 191-197, doi:10.1007/s40789-017-0169-y (2017).

33 Shao, J. F., Zhu, Q. Z. & Su, K. Modeling of creep in rock materials in terms of material degradation. *Comput Geotech* **30**, 549-555, doi:10.1016/S0266-352X(03)00063-6 (2003).

34 Aubertin, M., Gill, D. E. & Ladanyi, B. An internal variable model for the creep of rocksalt. *Rock Mech Rock Eng* **24**, 81-97, doi:10.1007/BF01032500 (1991).

35 Liu, C. & Li, H. Numerical simulation of realistic top coal caving intervals under different top coal thicknesses in longwall top coal caving working face. *Scientific Reports* **11**, 132-139, doi:10.1038/s41598-021-92624-y (2021).

36 Zhang, L. & Wang, X. Viscoelastic-plastic damage creep model for rock. *Chin J Geotech Eng* **42**, 1085-1092,

doi:10.11779/CJGE202006012 (2020).

37 Dhawan, H., Upadhyayula, S. & Sharma, D. K. Design of experiments to optimize the extraction parameters of a power grade Indian coal. *Int J Coal Sci Technol* **5**, 417-429, doi:10.1007/s40789-018-0216-3 (2018).